Multiphoton ionization in circularly polarized standing waves

Dong-Sheng Guo and G. W. F. Drake
Department of Physics, University of Windsor, Windsor, Ontario, Canada N9B 3P4
(Received 5 September 1991)

We derive the wave functions for an electron moving in a quantized circularly polarized standing-wave radiation field. By applying these solutions as the final states, we derive multiphoton ionization transition-rate formulas according to Keldysh-Faisal-Reiss (KFR) theory. Numerical calculations and theoretical analysis show that in the case of two light beams with the same angular momentum, KFR theory does not predict the peak splittings in the photoelectron angular distributions that were observed in an experiment by Bucksbaum, Schumacher, and Bashkansky (BSB) [Phys. Rev. Lett. **61**, 1162 (1988)]. A transition-rate formula from a scattering theory developed for the case of single-mode multiphoton ionization by Guo, Åberg, and Crasemann [Phys. Rev. A **40**, 4997 (1989)] is extended to the standing-wave case. The theory predicts the peak splitting observed by BSB. Numerical results of the splitting angle from the theory show good agreement with experimental measurements. We also prove that the sine function of the half splitting angle is inversely proportional to the square root of the photoelectron kinetic energy E, i.e., $\sin(\pi/2-\theta_{\max}) \propto 1/E^{1/2}$, where $\theta_{\max}$ is the maximum scattering angle smaller than $\pi/2$. Some predictions are made for future experimental observations, such as quantum effects associated with ponderomotive-energy decay.

PACS number(s): 32.80.Fb, 31.15.+q

I. INTRODUCTION

Recently, Bucksbaum, Schumacher, and Bashkansky [1] performed a multiphoton-ionization experiment using circularly polarized standing waves. They found an unusual peak splitting in the photoelectron angular distributions when the two light beams had the same angular momentum. They interpreted the effect as a Kapitza-Dirac effect [2] in a strong radiation field. This experimental result has not been well treated or interpreted in terms of a fundamental theory.

Experiments in multiphoton ionization play a very important role in studies of interactions between atoms and strong laser fields. The first experimental evidence [3] of multiphoton ionization was anticipated by the Keldysh-model theory [4], which when combined with later developments [5,6] is now often called Keldysh-Faisal-Reiss (KFR) theory. Although the KFR theory is controversial [7], it captures some important features of experimental measurements in multiphoton-ionization processes. It is therefore frequently used in the analysis of data [8]. Also, many subsequently developed theories are related to KFR theory [9–12]. Thus KFR theory still occupies an important position in theoretical discussions.

A standing wave can be thought of as a two-mode field of traveling waves. A recent development [13] in stationary solutions for an electron interacting with multimode photon fields has enabled us to extend the KFR theory to multimode cases [13]. From the general form of the multimode solutions we can write solutions for an electron interacting with standing waves. Two cases emerge, depending on whether the photon helicity vectors are antiparallel or parallel. The first case requires special treatment, while the second can be treated directly. Section II is devoted to obtaining these solutions for circularly polarized standing waves.

In Sec. III we extend the KFR theory to cases of standing-wave laser fields by applying these solutions as the final state of the electron while the initial state is the bound state to obtain a formula for the transition rate. A theoretical analysis and a numerical calculation using the extended KFR theory both show that the KFR theory does not predict the splitting of the angular-distribution peak found in the experiment of Bucksbaum and co-workers.

The principal aim of this paper is to show that a scattering theory for multiphoton ionization developed by Guo, Åberg, and Crasemann [10] and extended by us to multimode cases provides an explanation of the peak splitting in the angular distribution. In this theory, an extra transition bringing the electron from the inside to the outside of the radiation field is naturally and inevitably built in. In Sec. IV we present the extension of the scattering theory to the two-mode standing-wave case. Both theoretical analysis and numerical calculation predict the angular-distribution peak splitting when the two circularly polarized laser beams have the same angular momentum. Comparisons between the theoretical predictions and the experimental results of Bucksbaum and co-workers show good qualitative agreement and some quantitative agreement.

II. WAVE FUNCTIONS

The Hamiltonian for an electron moving in a standing-wave photon field can be written as

$$H=\frac{(-i\nabla)^2}{2m_e}-\frac{e}{2m_e}[(-i\nabla)\cdot\mathbf{A}_1(-\mathbf{k}\cdot\mathbf{r})+\mathbf{A}_1(-\mathbf{k}\cdot\mathbf{r})\cdot(-i\nabla)+(-i\nabla)\cdot\mathbf{A}_2(\mathbf{k}\cdot\mathbf{r})+\mathbf{A}_2(\mathbf{k}\cdot\mathbf{r})\cdot(-i\nabla)]$$
$$+\frac{e^2[\mathbf{A}_1(-\mathbf{k}\cdot\mathbf{r})+\mathbf{A}_2(\mathbf{k}\cdot\mathbf{r})]^2}{2m_e}+\omega N_{a_1}+\omega N_{a_2}\ , \tag{1}$$

where

$$\mathbf{A}_1(-\mathbf{k}\cdot\mathbf{r})=g(\boldsymbol{\epsilon}_1 e^{i\mathbf{k}\cdot\mathbf{r}}a_1+\boldsymbol{\epsilon}_1^* e^{-i\mathbf{k}\cdot\mathbf{r}}a_1^\dagger)\ ,$$
$$\mathbf{A}_2(\mathbf{k}\cdot\mathbf{r})=g(\boldsymbol{\epsilon}_2 e^{-i\mathbf{k}\cdot\mathbf{r}}a_2+\boldsymbol{\epsilon}_2^* e^{i\mathbf{k}\cdot\mathbf{r}}a_2^\dagger)\ ,\quad g=(2V_\gamma\omega)^{-1/2}\ , \tag{2}$$
$$N_{a_1}=\tfrac{1}{2}(a_1a_1^\dagger+a_1^\dagger a_1)\ ,$$
$$N_{a_2}=\tfrac{1}{2}(a_2a_2^\dagger+a_2^\dagger a_2)\ .$$

The eigenfunctions of this Hamiltonian can be found as follows.

The elliptical polarization vectors are defined by

$$\boldsymbol{\epsilon}_j=[\boldsymbol{\epsilon}_x\cos(\xi_j/2)+i\boldsymbol{\epsilon}_y\sin(\xi_j/2)]\exp(i\Theta_j/2)\ ,$$
$$\boldsymbol{\epsilon}_j^*=[\boldsymbol{\epsilon}_x\cos(\xi_j/2)-i\boldsymbol{\epsilon}_y\sin(\xi_j/2)]\exp(-i\Theta_j/2)\quad(j=1,2)\ . \tag{3}$$

After applying the transformation

$$\Psi(\mathbf{r})=e^{-i\mathbf{k}\cdot\mathbf{r}(N_{a_1}-N_{a_2})}\phi(\mathbf{r}) \tag{4}$$

and the transformation

$$\phi(\mathbf{r})=e^{i\mathbf{p}\cdot\mathbf{r}}\phi\ , \tag{5}$$

the eigenvalue equation for the Hamiltonian (1) becomes

$$\left[\frac{1}{2m_e}[\mathbf{p}-\mathbf{k}(N_{a_1}-N_{a_2})]^2-\frac{e}{2m_e}[\mathbf{p}\cdot(\mathbf{A}_1+\mathbf{A}_2)+(\mathbf{A}_1+\mathbf{A}_2)\cdot\mathbf{p}]+\frac{e^2(\mathbf{A}_1+\mathbf{A}_2)^2}{2m_e}+\omega N_{a_1}+\omega N_{a_2}\right]\phi=\mathcal{E}\phi\ , \tag{6}$$

where $\mathbf{k}\cdot\mathbf{A}_1=\mathbf{k}\cdot\mathbf{A}_2=0$ by transversality. Here, $\mathbf{A}_1$ and $\mathbf{A}_2$ are coordinate independent and defined by

$$\mathbf{A}_j=g(\boldsymbol{\epsilon}_j a_j+\boldsymbol{\epsilon}_j^* a_j^\dagger)\quad(j=1,2)\ . \tag{7}$$

We now make the following ansatz [13,14]: A real number κ can be defined such that $\mathbf{k}(N_{a_1}-N_{a_2})$ can be replaced by $\kappa\mathbf{k}$ with correction terms that are of order $v/c\simeq(2s\hbar\omega/m_ec^2)^{1/2}$, where s is the number of photons above threshold. For the experiment of Bucksbaum, Schumacher, and Bashkansky [1], one has $s\leq 13$ and $v/c\leq 0.07$. If we now define a vector $\mathbf{P}$ such that

$$\mathbf{p}=\mathbf{P}+\kappa\mathbf{k}\ , \tag{8}$$

then Eq. (6) is reduced to

$$\left[\frac{\mathbf{P}}{2m_e}-\frac{e}{m_e}\mathbf{P}\cdot(\mathbf{A}_1+\mathbf{A}_2)+\frac{e^2\mathbf{A}_1^2}{2m_e}+\frac{e^2\mathbf{A}_2^2}{2m_e}+\frac{e^2\mathbf{A}_1\cdot\mathbf{A}_2}{m_e}+\omega(N_{a_1}+N_{a_2})\right]\phi=\mathcal{E}\phi\ . \tag{9}$$

Equation (9) can be further written as

$$\left[\frac{\mathbf{P}^2}{2m_e}+H'_\gamma+V'\right]\phi=\mathcal{E}\phi\ , \tag{10}$$

where

$$H'_\gamma=(\omega+e^2g^2/m_e)(N_{a_1}+N_{a_2})\ ,$$
$$V'=-\frac{eg}{m_e}(\mathbf{P}\cdot\boldsymbol{\epsilon}_1a_1+\mathbf{P}\cdot\boldsymbol{\epsilon}_1^*a_1^\dagger)-\frac{eg}{m_e}(\mathbf{P}\cdot\boldsymbol{\epsilon}_2a_2+\mathbf{P}\cdot\boldsymbol{\epsilon}_2^*a_2^\dagger) \tag{11}$$
$$+\frac{e^2g^2}{m_e}(\boldsymbol{\epsilon}_1\cdot\boldsymbol{\epsilon}_2a_1a_2+\boldsymbol{\epsilon}_1^*\cdot\boldsymbol{\epsilon}_2^*a_1^\dagger a_2^\dagger)$$
$$+\frac{e^2g^2}{m_e}(\boldsymbol{\epsilon}_1\cdot\boldsymbol{\epsilon}_2^*a_1a_2^\dagger+\boldsymbol{\epsilon}_1^*\cdot\boldsymbol{\epsilon}_2a_1^\dagger a_2)\ .$$

In this paper, we mainly consider two important cases where the two constituent traveling beams are both circularly polarized.

Case I. Two beams with same angular momentum and opposite helicity. The easiest way to describe this case mathematically is to assume the following conditions:

$$\xi_1=\xi_2=\pi/2,\quad\Theta_1=\Theta_2=0\ , \tag{12}$$

which leads to

$$\boldsymbol{\epsilon}_1=\boldsymbol{\epsilon}_2\equiv\boldsymbol{\epsilon},\quad\boldsymbol{\epsilon}_1^*=\boldsymbol{\epsilon}_2^*\equiv\boldsymbol{\epsilon}^*\ , \tag{13}$$

and

$$\boldsymbol{\epsilon}\cdot\boldsymbol{\epsilon}^*=1,\quad\boldsymbol{\epsilon}\cdot\boldsymbol{\epsilon}=\boldsymbol{\epsilon}^*\cdot\boldsymbol{\epsilon}^*=0\ . \tag{14}$$

Thus, we have

$$H'_\gamma=(\omega+e^2g^2/m_e)(N_{a_1}+N_{a_2}) ,$$
$$V'=-\frac{eg}{m_e}[\mathbf{P}\cdot\boldsymbol{\epsilon}(a_1+a_2)+\mathbf{P}\cdot\boldsymbol{\epsilon}^*(a_1^\dagger+a_2^\dagger)] + \frac{e^2g^2}{m_e}(a_1a_2^\dagger+a_1^\dagger a_2) . \tag{15}$$

The general solutions that we obtained previously for two-mode cases [13] cannot be applied to this case, since it leads to a vanishing denominator in the general solutions. Thus we have to treat this as a special case as follows. To solve the Schrödinger equation, Eq. (10), we introduce a transformed photon representation with the two normal modes

$$c_1=\frac{1}{\sqrt{2}}(a_1+a_2),\quad c_1^\dagger=\frac{1}{\sqrt{2}}(a_1^\dagger+a_2^\dagger) ;$$
$$c_2=\frac{1}{\sqrt{2}}(a_1-a_2),\quad c_2^\dagger=\frac{1}{\sqrt{2}}(a_1^\dagger-a_2^\dagger) , \tag{16}$$

with the inverse

$$a_1=\frac{1}{\sqrt{2}}(c_1+c_2),\quad a_1^\dagger=\frac{1}{\sqrt{2}}(c_1^\dagger+c_2^\dagger) ;$$
$$a_2=\frac{1}{\sqrt{2}}(c_1-c_2),\quad a_2^\dagger=\frac{1}{\sqrt{2}}(c_1^\dagger-c_2^\dagger) . \tag{17}$$

The commutation relations for the new photon operators remain the same,

$$[c_1,c_1^\dagger]=[c_2,c_2^\dagger]=1 ,$$
$$[c_1,c_2]=[c_1^\dagger,c_2^\dagger]=[c_1,c_2^\dagger]=[c_2,c_1^\dagger]=0 . \tag{18}$$

The vacuum state also remains the same, since

$$c_1|0,0\rangle=0,\quad c_2|0,0\rangle=0 . \tag{19}$$

By the transformation, Eq. (17), we have the following relation:

$$a_1a_2^\dagger+a_1^\dagger a_2=\tfrac{1}{2}(c_1c_1^\dagger+c_1^\dagger c_1)-\tfrac{1}{2}(c_2c_2^\dagger+c_2^\dagger c_2) \equiv N_{c_1}-N_{c_2} , \tag{20}$$

which removes the energy degeneracy of H'_γ in Eq. (15). Thus we define

$$H''_\gamma=\left[\omega+2\frac{e^2g^2}{m_e}\right]N_{c_1}+\omega N_{c_2}\equiv\omega_1N_{c_1}+\omega N_{c_2} ,$$
$$V''=-\frac{eg\sqrt{2}}{m_e}(\mathbf{P}\cdot\boldsymbol{\epsilon}c_1+\mathbf{P}\cdot\boldsymbol{\epsilon}^*c_1^\dagger) , \tag{21}$$

and try to solve the equivalent Schrödinger equation

$$\left[\frac{\mathbf{P}^2}{2m_e}+H''_\gamma+V''\right]\phi=\mathcal{E}\phi . \tag{22}$$

From Eq. (21) we see that the interaction in Eq. (22) only involves the linear terms of c_1 and $c_1^\dagger$, and does not depend on the second normal mode. We also see that the first normal mode with the larger energy shift is due to the superposition of the two traveling waves with the same oscillation phase, and the second one without energy shift is due to the superposition with the opposite phase. In a classical picture, the first normal mode corresponds to points with maximum oscillation in the standing wave, and the second one corresponds to stationary points.

To eliminate the linear terms, we introduce a displacement operator

$$D_1=\exp(-\delta c_1^\dagger+\delta^*c_1) , \tag{23}$$

with

$$\delta=\frac{eg\sqrt{2}}{\omega_1m_e}\mathbf{P}\cdot\boldsymbol{\epsilon}^* , \tag{24}$$

which shifts the operators c_1, $c_1^\dagger$, and N_{c_1} according to

$$D_1c_1D_1^\dagger=c_1+\delta ,$$
$$D_1c_1^\dagger D_1^\dagger=c_1^\dagger+\delta^* , \tag{25}$$
$$D_1N_{c_1}D_1^\dagger=N_{c_1}+\delta^*c_1+\delta c_1^\dagger+\delta\delta^*$$

and changes the Hamiltonian $H''_\gamma+V''$ to

$$D_1(H''_\gamma+V'')D_1^\dagger=\omega_1N_{c_1}+\omega N_{c_2}-\frac{2e^2g^2(\mathbf{P}\cdot\boldsymbol{\epsilon})(\mathbf{P}\cdot\boldsymbol{\epsilon}^*)}{\omega_1m_e} . \tag{26}$$

Thus, we find solutions ϕ of Eq. (22) with the energy eigenvalue $\mathcal{E}$,

$$\phi=D_1^\dagger|n_1,n_2\rangle_c , \tag{27}$$

$$\mathcal{E}=\frac{\mathbf{P}^2}{2m_e}+(n_1+\tfrac{1}{2})\omega_1+(n_2+\tfrac{1}{2})\omega-\frac{2e^2g^2(\mathbf{P}\cdot\boldsymbol{\epsilon})(\mathbf{P}\cdot\boldsymbol{\epsilon}^*)}{\omega_1m_e} .$$

With the condition of a strong radiation field, we can take the large-photon-number limit for the above solutions [13,15]. We let n_1 and n_2 become large, and g become small, such that $g\sqrt{n_1}\to\Lambda$ and $g\sqrt{n_2}\to\Lambda$; then,

$$\phi=\sum_{m_1,m_2}|m_1,m_2\rangle_c\langle m_1,m_2|_cD_1^\dagger|n_1,n_2\rangle_c$$
$$=\sum_{m_2j}|n_1+j,m_2\rangle_c\langle n_1+j|_cD_1^\dagger|n_1\rangle_c\delta_{m_2n_2}$$
$$\to\sum_j|n_1+j,n_2\rangle_c(-1)^jJ_j(\xi)e^{-ij\varphi} , \tag{28}$$

where

$$\varphi=\arctan(P_y/P_x)$$
$$\xi=\frac{2\sqrt{2}|e|\Lambda}{m_e\omega}|\mathbf{P}\cdot\boldsymbol{\epsilon}| . \tag{29}$$

The limiting form for the energy eigenvalues is

$$\mathcal{E}=\frac{\mathbf{P}^2}{2m_e}+(n_1+\tfrac{1}{2})\omega+(n_2+\tfrac{1}{2})\omega+2z\omega , \tag{30}$$

where

$$z=\frac{e^2\Lambda^2}{m_e\omega} , \tag{31}$$

with $z\omega$ being the ponderomotive potential for each original mode.

To determine the value for $\kappa\mathbf{k}\equiv\mathbf{p}-\mathbf{P}$, we assume that the constituent two traveling waves have the same intensity, and thus the same background-photon number and ponderomotive potential energy. In the general two-mode case we have

$$\mathbf{p}-\mathbf{P}=(l_1+\tfrac{1}{2})\mathbf{k}_1+(l_2+\tfrac{1}{2})\mathbf{k}_2+z_1\mathbf{k}_1+z_2\mathbf{k}_2 , \tag{32}$$

where l_1 and l_2 are the background-photon numbers for the two modes. Under the equal-intensity assumption, for the case of standing waves we have

$$\mathbf{p}-\mathbf{P}=\mathbf{0} . \tag{33}$$

Finally, the eigenfunctions for the Hamiltonian under the assumed conditions are

$$\Psi(\mathbf{r})= V_e^{-1/2}e^{i[\mathbf{P}-\mathbf{k}(N_{a_1}-N_{a_2})]\cdot\mathbf{r}} \times\sum_j |n_1+j,n_2\rangle_c J_{-j}(\zeta)e^{-ij\varphi} . \tag{34}$$

Case II. Two beams with the same helicity and opposite angular momentum. This case is described by

$$\xi_1=-\xi_2=\pi/2, \quad \Theta_1=\Theta_2=0 , \tag{35}$$

which leads to

$$\boldsymbol{\epsilon}_1=\boldsymbol{\epsilon}_2^*\equiv\boldsymbol{\epsilon}, \quad \boldsymbol{\epsilon}_1^*=\boldsymbol{\epsilon}_2\equiv\boldsymbol{\epsilon}^* , \tag{36}$$

and

$$\boldsymbol{\epsilon}\cdot\boldsymbol{\epsilon}^*=1, \quad \boldsymbol{\epsilon}\cdot\boldsymbol{\epsilon}=\boldsymbol{\epsilon}^*\cdot\boldsymbol{\epsilon}^*=0 . \tag{37}$$

Thus we have

$$H'_\gamma=(\omega+e^2g^2/m_e)(N_{a_1}+N_{a_2}) , \tag{38}$$

$$V'=-\frac{eg}{m_e}(\mathbf{P}\cdot\boldsymbol{\epsilon}_1a_1+\mathbf{P}\cdot\boldsymbol{\epsilon}_1^*a_1^\dagger)-\frac{eg}{m_e}(\mathbf{P}\cdot\boldsymbol{\epsilon}_2a_2+\mathbf{P}\cdot\boldsymbol{\epsilon}_2^*a_2^\dagger) +\frac{e^2g^2}{m_e}(a_1a_2+a_1^\dagger a_2^\dagger) .$$

Solutions for this case can be treated as special cases of the general two-mode solutions [13]. According to the general solutions, the singular term appearing in case I does not arise in this case because of Eqs. (36) and (37). Thus the wave functions can be written directly as

$$\Psi_{\mathbf{P}n_1n_2}(\mathbf{r})=V_e^{-1/2}e^{i\mathbf{P}\cdot\mathbf{r}}\sum_{j_1j_2} |n_1+j_1,n_2+j_2\rangle\mathscr{J}_{j_1j_2}(\zeta)^* \times e^{-i(j_1-j_2)(\mathbf{k}\cdot\mathbf{r}+\varphi)} . \tag{39}$$

The generalized Bessel functions are defined as

$$\mathscr{J}_{j_1j_2}(\zeta)=\sum_q J_{-j_1+q}(\zeta_1)J_{-j_2+q}(\zeta_1)J_{-q}(\zeta_5) , \tag{40}$$

where

$$\zeta_1=\frac{2|e|\Lambda}{m_e\omega}|\mathbf{P}\cdot\boldsymbol{\epsilon}|, \quad \zeta_5=z=\frac{e^2\Lambda^2}{m_e\omega} . \tag{41}$$

The energies are

$$\mathscr{E}=\frac{\mathbf{P}^2}{2m_e}+(n_1+\tfrac{1}{2})\omega+(n_2+\tfrac{1}{2})\omega+2z\omega , \tag{42}$$

which is the same as Eq. (30) for case I.

III. TRANSITION RATE IN KELDYSH-FAISAL-REISS THEORY

KFR theory is the most popular nonperturbative theory for multiphoton ionization. Even though its range of validity is not well established, it has made an important historical contribution to the understanding of the nonperturbative features of multiphoton ionization. In KFR theory, the initial state of the electron is an atomic bound state, while the final state is assumed to be a time-dependent semiclassical Volkov state in which the electron is assumed to move in a classical radiation field. The transition rate for multiphoton ionization in KFR theory can be derived as the leading term of a two-potential theory in which the interaction between the electron and the radiation field is treated nonperturbatively, while the interaction between the electron and the atomic Coulomb field is treated perturbatively [4,12], but without adiabatic switching off of the radiation field for the final state. It has also been proven that KFR theory can be derived by a fully quantum-mechanical and time-independent formalism in which the initial state is assumed to be an atomic bound state while the final state is a quantum-field Volkov state—a state for an electron and a group of photons interacting together [10,15]. By adopting the latter approach, we can use the exact wave functions derived in Sec. II as the final states for both the photoelectron and the standing-wave photon field to derive the transition rate for multiphoton ionization in a circularly polarized strong standing-wave laser field.

The initial state for the bound electron and the free photon field in a standing wave is described by

$$|\Phi_i(\mathbf{r});l,l\rangle=\Phi_i(\mathbf{r})|l,l\rangle , \tag{43}$$

where we assume that the constituent traveling photon beams have the same intensity, and therefore the same photon number l.

Case I. Two beams with same angular momentum and opposite helicity. The final-state wave function is described by Eq. (34). The following steps can help to avoid lengthy calculations. The KFR transition matrix element can be written as

$$T_{fi}=\langle\Psi_f(\mathbf{r})|V(\mathbf{r})|\Phi_i(\mathbf{r});l,l\rangle =V_e^{-1/2}\sum_s J_{-s}(\zeta)e^{is\varphi}\langle n_1+s,n_2|_cV|l,l\rangle\Phi_i(\mathbf{P}) , \tag{44}$$

where

$$V=e^{-i[\mathbf{P}-\mathbf{k}(N_{a_1}-N_{a_2})]\cdot\mathbf{r}}V(\mathbf{r})e^{i[\mathbf{P}-\mathbf{k}(N_{a_1}-N_{a_2})]\cdot\mathbf{r}}$$

$$=-\frac{e}{m_e}\mathbf{P}\cdot(\mathbf{A}_1+\mathbf{A}_2)+\frac{e^2(\mathbf{A}_1+\mathbf{A}_2)^2}{2m_e} . \tag{45}$$

By introducing

$$H_\gamma=\omega(N_{a_1}+N_{a_2}) \tag{46}$$

and noticing that H_γ and V are both pure photon operators, which are Hermitian, we have

$$T_{fi}=V_e^{-1/2}\sum_s J_{-s}(\zeta)e^{is\varphi}\langle n_1+s,n_2|_c(H_\gamma+V)-H_\gamma|l,l\rangle \times\Phi_i(\mathbf{P})$$
$$=V_e^{-1/2}\delta\mathcal{E}\sum_s J_{-s}(\zeta)e^{is\varphi}\langle n_1+s,n_2|_c l,l\rangle\Phi_i(\mathbf{P}) , \tag{47}$$

where $\delta\mathcal{E}$ is an energy difference defined as

$$\delta\mathcal{E}=[(n_1+\tfrac{1}{2})\omega+(n_2+\tfrac{1}{2})\omega+2z\omega]-(2l+1)\omega \equiv 2z\omega-j\omega , \tag{48}$$

and

$$j\equiv 2l-n_1-n_2 \tag{49}$$

is the transferred photon number (i.e., the difference between the initial free photon number $2l$ and the intermediate background-photon number n_1+n_2). The factor of the inner product in Eq. (47) can be evaluated algebraically according to

$$\langle n_1+s,n_2|_c l,l\rangle=2^{-l}(n!)^{-1}\langle n_1+s,n_2|_c(c_1^{\dagger 2}-c_2^{\dagger 2})^l|0,0\rangle$$
$$=(-1)^{n_2/2}2^{-l}\begin{bmatrix}2l-n_2\\ l-n_2/2\end{bmatrix}^{1/2}\begin{bmatrix}n_2\\ n_2/2\end{bmatrix}^{1/2} \times\delta_{n_1+n_2+s,2l} \tag{50}$$

for n_2 even, and $\langle n_1+s,n_2|_c l,l\rangle=0$ for n_2 odd. Summing the squares of the transition matrix elements over all final states yield

$$\sum_f|T_{fi}|^2=V_e^{-1}\omega^2(j-2z)^2J_j^2(\zeta)|\Phi_i(\mathbf{P})|^2 \times\left[2^{-2l}\sum_{n_2}\begin{bmatrix}2l-n_2\\ l-n_2/2\end{bmatrix}\begin{bmatrix}n_2\\ n_2/2\end{bmatrix}\right] . \tag{51}$$

The sum over all final states simplifies since only even values of n_2 contribute. In this case the combinatorial identity [16]

$$\sum_q\begin{bmatrix}2l-2q\\ l-q\end{bmatrix}\begin{bmatrix}2q\\ q\end{bmatrix}=2^{2l} \tag{52}$$

shows that the factor in the large square brackets in (51) is equal to 1.

After integrating over the radial part of momentum space and imposing the energy conservation condition [13,15]

$$\frac{\mathbf{P}^2}{2m_e}=j\omega-2z\omega-E_b , \tag{53}$$

where E_b is the binding energy of the initial bound state, we finally obtain the transition-rate formula

$$\frac{dw}{d\Omega}=\int_0^\infty V_e(2\pi)^{-3}\mathbf{P}^2d|\mathbf{P}|\,|T_{fi}|^2_{\rm av}2\pi \times\delta\left[\frac{\mathbf{P}^2}{2m_e}-j\omega+2z\omega+E_b\right]$$
$$=\frac{(2m_e^3\omega^5)^{1/2}}{(2\pi)^2}(j-2z)^2(j-2z-E_b/\omega)^{1/2} \times|\Phi_i(\mathbf{P})|^2_{\rm av}J_j^2(\zeta) . \tag{54}$$

The subscript av on the square of the transition matrix element and the momentum wave function means the average value over initial states with the same principle quantum number and orbital angular quantum number, but with different magnetic quantum numbers. The average of the square of the Fourier transform can be simplified to a pure radial integral [13] with no angular dependence.

Equation (54) clearly shows that there is no peak splitting in the angular distribution. The reason is as follows. The angular distribution only depends on the Bessel function part, which is a locally monotonic function of ζ. From Eq. (29), one can see that the peak value occurs when the scattering angle is $\pi/2$. The rate formula, Eq. (54), is exactly the same as that for a single-mode traveling-wave case with the same total intensity if one neglects retardation effects on the single-mode traveling wave. The total ponderomotive potential energies are the same in the two cases, since the total intensities are the same and these quantities obey the law of linear superposition [14].

To compare the theoretical results with experimental measurements, we choose xenon as the model atom for calculations. The outermost shell of a Xenon atom is $5p_{3/2}$. The radial wave function for the $5p_{3/2}$ electron is obtained by taking the large component of the same orbital generated by fitting all energy levels of a relativistic electron in a Tietz model potential [17] to those of xenon. Figure 1 shows the calculated angular distribution for case I. The assumed conditions correspond to 15-photon ionization with an intensity of 10^{13} W/cm^2 and a wave-

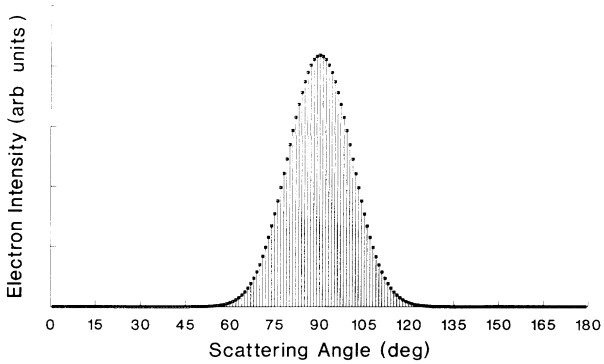

FIG. 1. Angular distribution for the photoelectron in case I, calculated from the extended KFR theory.

length of 1064 nm for each traveling beam. One can see that there is no peak splitting in the angular distribution.

Case II. Two beams with the same helicity and opposite angular momentum. The general formalism applies to this case, so we can write the transition-rate formula directly from the general two-mode theory of the KFR type for multiphoton ionization [13]. The transition rate for an electron absorbing j_1 photons from the first mode and j_2 photons from the second mode is

$$\frac{dw}{d\Omega}=\frac{(2m_e^3\omega^5)^{1/2}}{(2\pi)^2}(j_1+j_2-2z)^2(j_1+j_2-2z-E_b/\omega)^{1/2} \times|\Phi_i[\mathbf{P}-(j_1-j_2)\mathbf{k}]|^2_{\mathrm{av}}|\mathscr{I}_{j_1j_2}(\zeta)|^2 . \quad (55)$$

Energy conservation in this case gives

$$\frac{\mathbf{P}^2}{2m_e}=(j_1+j_2)\omega-2z\omega-E_b , \quad (56)$$

from which we can see that the energy peak position of the photoelectron depends on j_1+j_2, not on j_1 and j_2 separately. Thus, for a certain energy peak corresponding to absorbing a total of j photons, the transition rate is

$$\left[\frac{dw}{d\Omega}\right]_j=\sum_{j_1,j_2}\frac{dw}{d\Omega}\delta_{j,j_1+j_2} . \quad (57)$$

Figure 2 shows the calculated angular distribution for case II, assuming the same condition as above. One can see that the angular distribution has a more complicated shape. Mathematically, the oscillations are due to the nonmonotonic property of the generalized Bessel functions with respect to the argument ζ_1, which is proportional to $\sin\vartheta$. The generalized Bessel functions in this case are combinations of three single Bessel functions. When ζ_1 passes through a point of local maximum value for the generalized Bessel function before ϑ reaches $\pi/2$, peaks with sidebands occur. It should be emphasized that this kind of shape has nothing to do with the peak splitting of Bucksbaum and co-workers observed in case I. The shapes are a mathematical property of the generalized Bessel functions, and oscillations may not always occur as one varies the input parameters in the calculation.

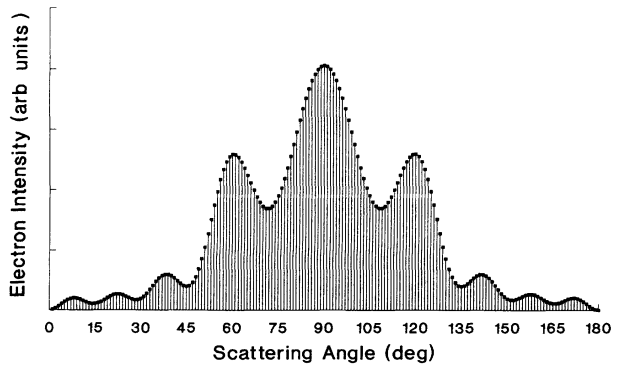

FIG. 2. Angular distribution for the photoelectron in case II, calculated from the extended KFR theory.

IV. TRANSITION RATE FROM SCATTERING THEORY

Guo, Åberg, and Crasemann (GAC) developed a scattering theory for multiphoton ionization by applying a formal scattering theory [10]. In the GAC theory, the leading term of the final state in a perturbation expansion of the atomic Coulomb potential can be expressed as

$$\Psi_f^-=\sum_\mu|\Psi_\mu\rangle\langle\Psi_\mu|\phi_f,m\rangle \quad (\mathscr{E}_\mu=\mathscr{E}) , \quad (58)$$

where $|\phi_f,m\rangle$ is a plane wave for the electron-photon system with ϕ_f being an electron plane wave and $|m\rangle$ a number state of m free photons. The $|\Psi_\mu\rangle$ are the time-independent quantized-field Volkov states having the same energy eigenvalue $\mathscr{E}$ as the final plane-wave state $|\phi_f,m\rangle$. The Ψ_μ are the *on-shell intermediate states.* Since the photoelectrons are collected under conditions where there are no surrounding external radiation fields, Eq. (58) should provide a better description of the photoelectron than KFR theory provides. A complication of theory is that the final state is defined only when z is an integer, where z is the number of ponderomotive photons. This peculiar conclusion should be no problem for cases of high-intensity fields, where z is a large number, but it is not adequate when z is only a small and noninteger number. The difficulty arises from the single-mode assumption for the interaction. In quantum electrodynamics, the photon field operator includes all possible photon modes. Even if the initial state were a perfect single-mode photon state, extra photon modes could still be created through a scattering process, if energy and momentum conservation were satisfied. The treatment could be refined by adding extra modes to the interaction term in the Hamiltonian, such that spontaneous emission of those extra modes would balance four-momentum conservation. In this treatment, if four-momentum conservation is not satisfied, there must be some spontaneous emission involved in the actual process. In the case of standing-wave multiphoton ionization, the situation is better than in a single-mode case, since four-momentum conservation can be more easily satisfied between two electron states and the two photon beams. In this paper, for simplicity, we will not include the spontaneous-emission modes in the interaction. Rather, we leave them for a later detailed treatment. Here we extend the GAC theory to the case of two-mode standing waves. The corresponding final state is

$$\Psi_f^-=\sum_\mu|\Psi_\mu\rangle\langle\Psi_\mu|\phi_f;m_1,m_2\rangle \quad (\mathscr{E}_\mu=\mathscr{E}) , \quad (59)$$

where $|m_1,m_2\rangle$ is a free photon state with photon number m_1 and m_2 for each mode and ϕ_f is the electron plane wave with momentum $\mathbf{P}$, i.e.,

$$|\phi_f;m_1,m_2\rangle=V_e^{-1/2}e^{i\mathbf{P}\cdot\mathbf{r}}|m_1,m_2\rangle , \quad (60)$$

while the Ψ_μ are all possible states obtained in Sec. II,

with the same energy eigenvalue as the plane wave $|\phi_f;m_1,m_2\rangle$. Using Eq. (59) as the final state, the transition matrix element is

$$T_{fi}=\sum_{\mu}\langle\phi_f;m_1,m_2|\Psi_\mu\rangle T_{\mu i}^{\mathrm{KFR}} , \tag{61}$$

where $T_{\mu i}^{\mathrm{KFR}}$ is the transition matrix element in KFR theory.

Case I. Two beams with the same angular momentum and opposite helicity. Using the solution, Eq. (34), the overlap factor in Eq. (61) is

$$\begin{aligned}\langle\phi_f;m_1,m_2|\Psi_\mu\rangle &= V_e^{-1}\langle m_1,m_2|e^{-i\mathbf{P}\cdot\mathbf{r}}e^{i[\mathbf{P}_\mu-\mathbf{k}(N_{a_1}-N_{a_2})]\cdot\mathbf{r}}\sum_s|n_1+s,n_2\rangle_c J_{-s}(\zeta)e^{-is\varphi}\\ &=(2\pi)^3\mathbf{V}_e^{-1}\sum_s\langle m_1,m_2|n_1+s,n_2\rangle_c J_{-s}(\zeta)e^{-is\varphi}\delta(\mathbf{P}_\mu-\mathbf{P}+(m_2-m_1)\mathbf{k}) .\end{aligned} \tag{62}$$

Combining the energy conservation equation

$$\frac{1}{2m_e}\mathbf{P}_\mu^2+(n_1+\tfrac{1}{2})\omega+(n_2+\tfrac{1}{2})\omega+2z\omega = \frac{\mathbf{P}^2}{2m_e}+(m_1+\tfrac{1}{2})\omega+(m_2+\tfrac{1}{2})\omega , \tag{63}$$

with the momentum conservation expressed by the δ function in Eq. (62)

$$\mathbf{P}_\mu=\mathbf{P}-(m_2-m_1)\mathbf{k} , \tag{64}$$

we get a quadratic equation for m_2-m_1

$$(m_2-m_1)^2-2(m_2-m_1)|\mathbf{P}|\omega^{-1}\cos\vartheta+2m_e\omega^{-1}(2z-j')=0 , \tag{65}$$

where

$$j'\equiv m_1+m_2-(n_1+n_2) \tag{66}$$

and ϑ is the polar angle of $\mathbf{P}$, or the scattering angle for the photoelectron. The quantity m_2-m_1 is the photon-number difference between the two modes in the final plane wave, which may be called the *mode-change quantum number.*

To see the physics more clearly, let us try an approximate solution for m_2-m_1 first by solving the following equation, which is also from Eqs. (63) and (64):

$$(m_2-m_1)^2+2(m_2-m_1)|\mathbf{P}_\mu|\omega^{-1}\cos\vartheta_\mu-2m_e\omega^{-1}(2z-j')=0 , \tag{67}$$

where ϑ_μ is the polar angle of $\mathbf{P}_\mu$. The momentum $\mathbf{P}_\mu$ refers to the Volkov-type intermediate states. The transition amplitude from the initial bound state to the states of Volkov type is the KFR transition matrix, which produces a peak at $\vartheta_\mu=\pi/2$ in angular distribution (Fig. 1). Thus we can let the middle term of Eq. (67) be zero to obtain the approximate values for m_2-m_1

$$m_2-m_1\approx\pm[2m_e\omega^{-1}(2z-j')]^{1/2} , \tag{68}$$

which is exact at the peak point of the angular distribution. Thus we get the constraint for j',

$$j'=0,1,2,\ldots,\le 2z . \tag{69}$$

If we notice that $2z\omega$ is the total ponderomotive energy of the field, the physical meaning of j' becomes immediately clear. The integer j' corresponds to the conversion of ponderomotive potential energy into j' photons of energy ω. When the electron leaves the field, it does not keep all its ponderomotive potential energy if $j'\neq 0$, but returns j' photons to the background field, as shown by Eq. (66). The maximum ponderomotive decay is at $j'=[2z]$, the largest integer smaller than $2z$. In the $j'=0$ case, the electron keeps all its ponderomotive potential energy. The mode-change quantum number gives the peak splitting in angular distribution. Equation (68) shows that the peak splitting observed by Bucksbaum, Schumacher, and Bashkansky (BSB) is due to the ponderomotive potential energy gained by the photoelectron. The largest splitting angle occurs for the $j'=0$ case.

The solutions of Eq. (65) are

$$m_2-m_1=|\mathbf{P}|\omega^{-1}\cos\vartheta\pm[|\mathbf{P}|^2\omega^{-2}\cos^2\vartheta-2m_e\omega^{-1}(2z-j')]^{1/2} , \tag{70}$$

where, from Eq. (63),

$$|\mathbf{P}|=[|\mathbf{P}_\mu|^2+2m_e\omega(2z-j')]^{1/2}\quad(\mu=1,2) . \tag{71}$$

Unlike the single-mode case where μ has only one value [10], we know from Eq. (65) that μ can now have two values. The $\mathbf{P}_1$ and $\mathbf{P}_2$ are different only in direction. They have the same norm shown by Eq. (53), which expresses energy conservation for the KFR transition,

$$|\mathbf{P}_\mu|=[2m_e(j\omega-2z\omega-E_b)]^{1/2}\quad(\mu=1,2) . \tag{72}$$

Here, j is the absorbed-photon number to excite the electron into a Volkov-type state. Thus we have a direct expression for $|\mathbf{P}|$,

$$|\mathbf{P}|=[2m_e(j\omega-j'\omega-E_b)]^{1/2} . \tag{73}$$

Figure 3(a) shows the geometric relations between $\mathbf{P}$ and $\mathbf{P}_\mu$ ($\mu=1,2$), 3(b) shows the geometric relation when $\mathbf{P}$ has the maximum polar angle, which determines the peak splitting in the angular distribution. For fixed j and j', the maximum polar angle smaller than $\pi/2$ can be easily obtained from the geometric relation shown in the graph,

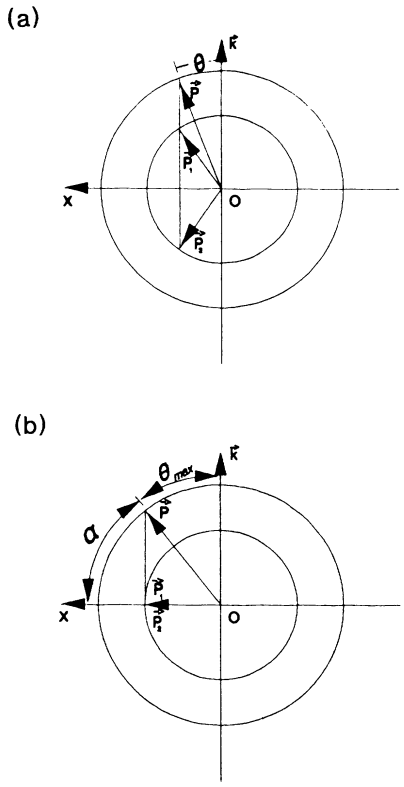

FIG. 3. (a) Geometric relation between the momentum of the on-shell intermediate Volkov states and that of the final plane wave. (b) Geometric relation in the case of the maximum scattering angle, which determines the splitting angle.

$$\vartheta_{\max}=\arcsin|\mathbf{P}_1|/|\mathbf{P}|$$
$$=\arcsin[(j-2z-E_b/\omega)/(j-j'-E_b/\omega)]^{1/2} . \quad (74)$$

The half spitting angle α from the geometric relation reduces to

$$\alpha\equiv\pi/2-\vartheta_{\max}$$
$$=\arcsin[(2z-j')/(j-j'-E_b/\omega)]^{1/2} . \quad (75)$$

Since the above numerator is a fixed number for some particular j', we have the following inverse square-root law for $\sin\alpha$:

$$\sin\alpha\propto 1/\sqrt{E} , \quad (76)$$

where

$$E=\frac{\mathbf{P}^2}{2m_e}=j\omega-j'\omega-E_b \quad (77)$$

is the kinetic energy of the photoelectron after the ponderomotive potential scattering. This is the true final kinetic energy observed by the electron energy spectrometer. In their measurement, BSB obtained ten values for α at five different photoelectron energies. As shown in Fig. 4, a least-squares fit to a function of the form

$$\sin\alpha=aE^b \quad (78)$$

yields $a=0.947\pm0.04$ eV^{-b} and $b=-0.47\pm0.09$, in agreement with $a=0.965$ eV$^{1/2}$ from Eq. (75) and $b=-\frac{1}{2}$ from Eq. (76). Figure 4 compares the theoretical curve with the least-squares fit to the data.

We next investigate the detailed structure of the differential ionization rate. The overlap factor in Eq. (62) can be further evaluated,

$$\langle m_1,m_2|n_1+s,n_2\rangle_c$$
$$=\left[\frac{m_1!m_2!}{2^{n_1+n_2+s}(n_1+s)!n_2!}\right]^{1/2}\delta_{m_1+m_2,n_1+n_2+s}$$
$$\times\sum_t(-1)^t\begin{bmatrix}n_1+s\\m_2-t\end{bmatrix}\begin{bmatrix}n_2\\t\end{bmatrix} . \quad (79)$$

Equations (49), (66), and (79) show that the total photon number of the final state must be

$$m_1+m_2=2l-(j-j') . \quad (80)$$

Combining this relation with Eq. (70), we know that the pair (m_1,m_2) can only have two values corresponding to the two values of $\mathbf{P}_\mu$ ($\mu=1,2$). Thus we see that the index μ indicates different final plane-wave states, rather than the different on-shell intermediate states. The angular distribution of the transition rate is obtained by integrating the square of the transition matrix element over $|\mathbf{P}|$ and summing over μ, for fixed j and j',

$$\frac{dw}{d\Omega}=\frac{(2m_e^3\omega^5)^{1/2}}{(2\pi)^2}(j-2z)^2(j-j'-E_b/\omega)^{1/2}$$
$$\times[|\Phi_i(\mathbf{P}_1)|^2_{\rm av}F_1^2+|\Phi_i(\mathbf{P}_2)|^2_{\rm av}F_2^2]J_j^2(\zeta)J_{j'}^2(\zeta) , \quad (81)$$

where

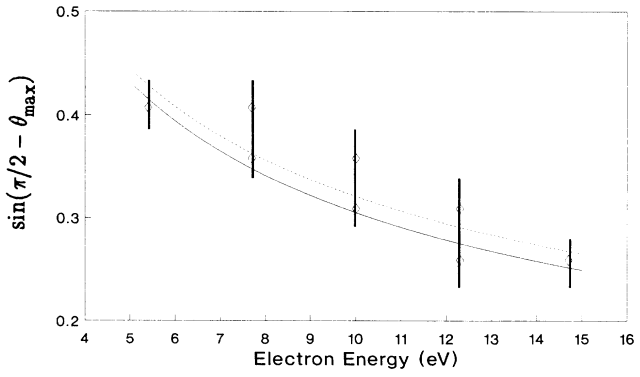

FIG. 4. Relation between $\sin(\pi/2-\theta_{\max})$ and the photoelectron energy E. The dashed curve is the least-squares fit to the ten measured data points ($\Diamond$). The least-squares fit is proportional to $1/E^{0.47}$. The solid curve corresponds to the predicted $\sin(\pi/2-\theta_{\max})\propto 1/E^{1/2}$ law. The laser intensity per beam used in the calculation is 2.1×10^{13} W/cm^2.

$$\zeta=\frac{2\sqrt{2}|e|\Lambda}{m_e\omega}|\mathbf{P}\cdot\boldsymbol{\epsilon}|$$
$$=\frac{2\sqrt{2}|e|\Lambda}{m_e\omega}|\mathbf{P}_1\cdot\boldsymbol{\epsilon}|=\frac{2\sqrt{2}|e|\Lambda}{m_e\omega}|\mathbf{P}_2\cdot\boldsymbol{\epsilon}| \ . \tag{82}$$

In obtaining Eq. (81), we have applied the relation shown by Eq. (82). The two factors F_1 and F_2 can be written in one expression according to the two groups of values of (m_1,m_2) obtained by Eqs. (70) and (80),

$$F=\sum_{n_2}\left[\frac{m_1!m_2!}{2^{m_1+m_2}(m_1+m_2-n_2)!n_2!}\right]^{1/2}$$
$$\times\left[\sum_t(-1)^t\begin{pmatrix}m_1+m_2-n_2\\ m_2-t\end{pmatrix}\begin{pmatrix}n_2\\ t\end{pmatrix}\right]$$
$$\times(-1)^{n_2/2}2^{-l}\left[\begin{pmatrix}2l-n_2\\ l-n_2/2\end{pmatrix}\begin{pmatrix}n_2\\ n_2/2\end{pmatrix}\right]^{1/2}, \tag{83}$$

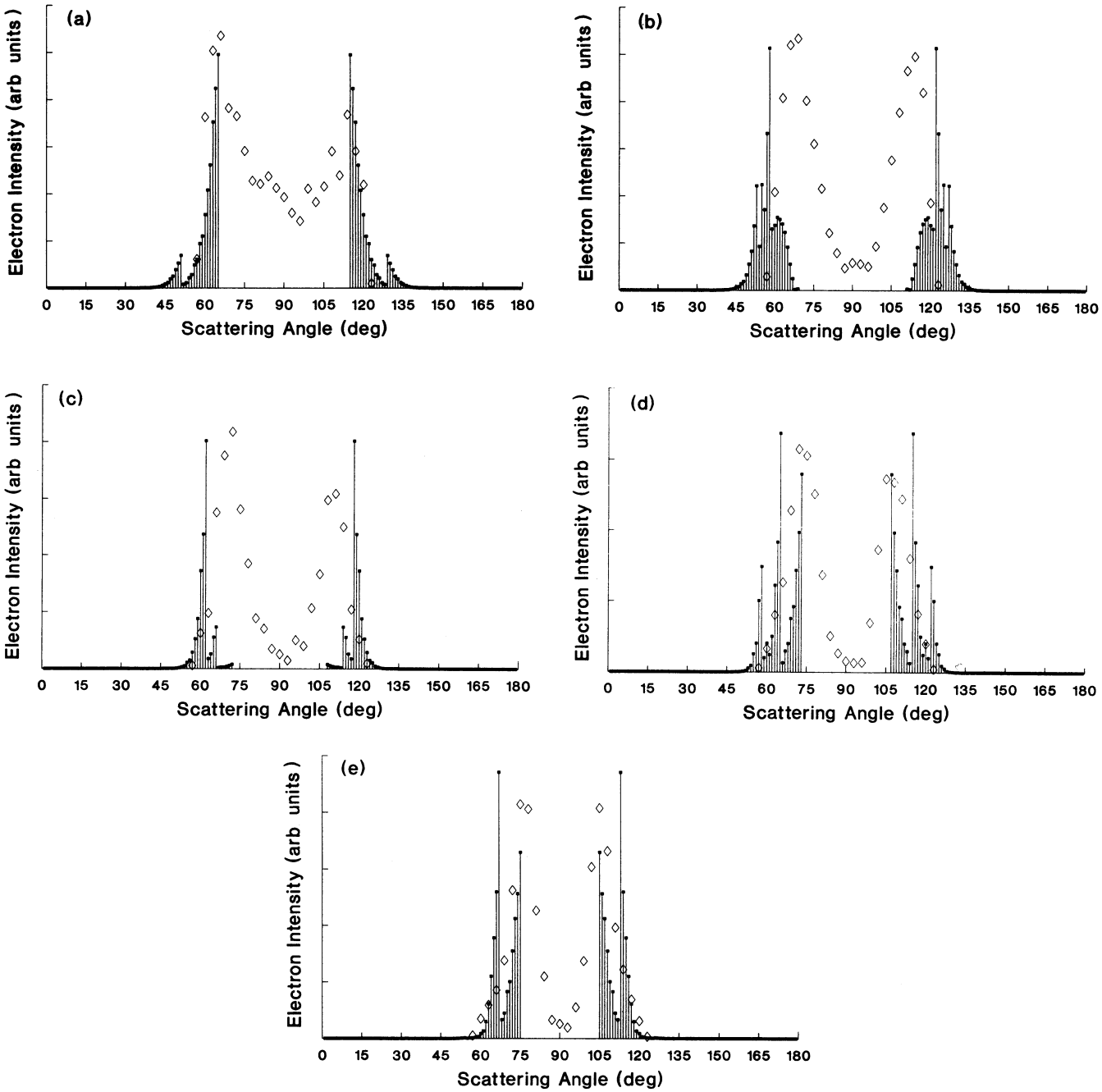

FIG. 5. Angular distributions for the photoelectron in the (a) 15-, (b) 17-, (c) 19-, (d) 21-, and (e) 23-photon ionization cases calculated at an intensity of 1×10^{13} W/cm^2 per beam and comparisons with the measurements (◇) of Bucksbaum and co-workers. The theoretical results are marked by vertical lines, with the vertical scale in arbitrary units.

which is a pure number, independent of n_1, j, and j'. In the large-photon-number limit, the factor F approaches the simple expression,

$$F=\frac{2}{\pi\Delta} , \tag{84}$$

where

$$\Delta=m_2-m_1 \tag{85}$$

is the photon-number difference between the two modes of the final state, i.e., the mode-change quantum number. The proof is given in the Appendix.

The average of the square of the Fourier transforms only depends on the absolute values of $\mathbf{P}_1$ and $\mathbf{P}_2$ [13], which are the same by Eq. (72), so the two terms in Eq. (81) can be combined. We have the final form

$$\frac{dw}{d\Omega}=\frac{(2m_e^3\omega^5)^{1/2}}{(2\pi)^2}(j-2z)^2(j-j'-E_b/\omega)^{1/2} \times|\Phi_i(\mathbf{P}_1)|^2_{\mathrm{av}}(F_1^2+F_2^2)J_j^2(\zeta)J_{j'}^2(\zeta) . \tag{86}$$

From Eq. (77) we can see that $j-j'$ is the total

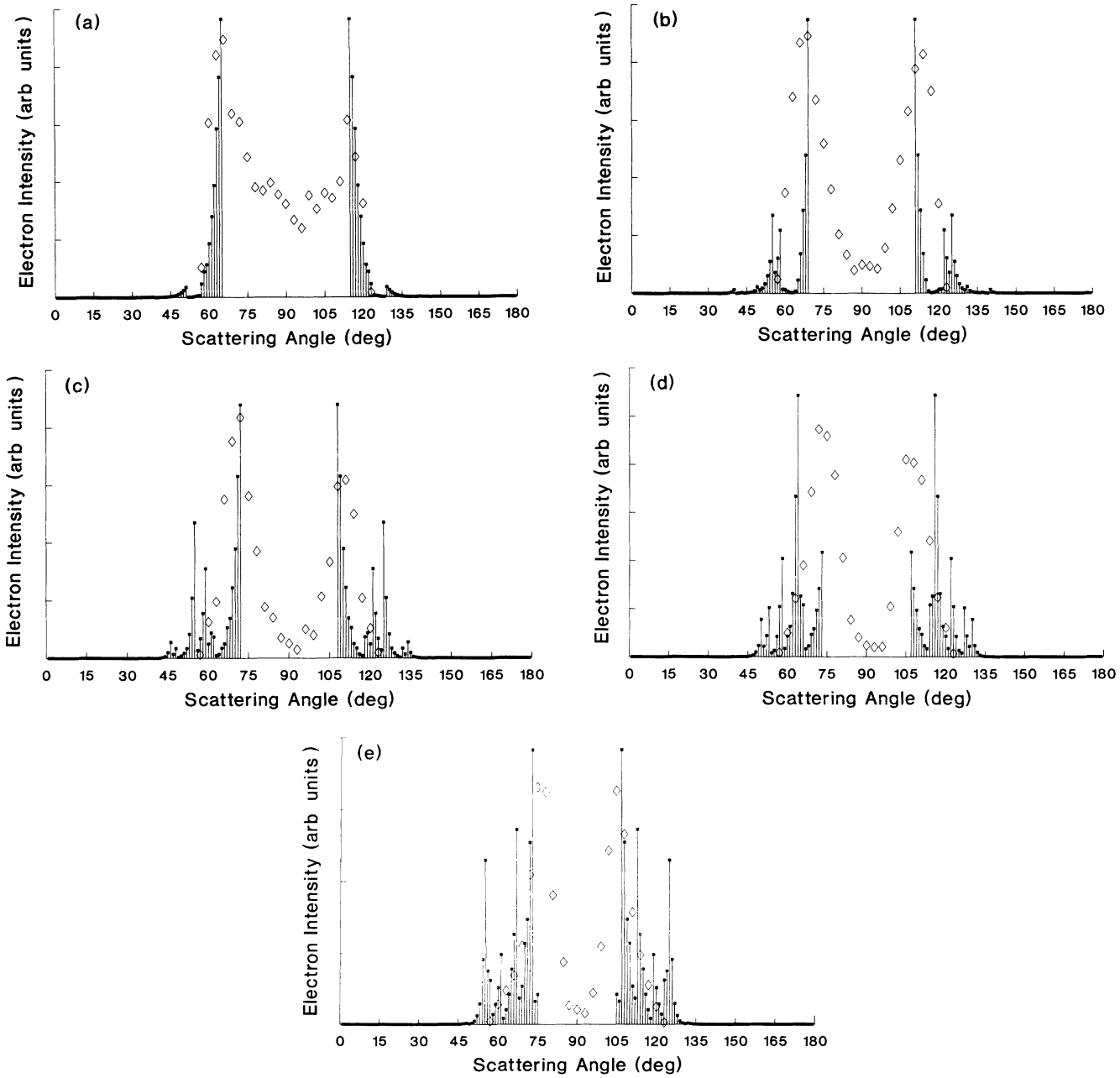

FIG. 6. Angular distributions for the photoelectron in the (a) 15-, (b) 17-, (c) 19-, (d) 21-, and (e) 23-photon ionization cases calculated at an intensity of 2.1×10^{13} W/cm^2 per beam and comparisons with the measurements (◇) of Bucksbaum and co-workers.

absorbed-photon number. For the same photoelectron kinetic energy, $j-j'$ should be the same, but j and j' may be different. This reveals that multiphoton ionization may go through different channels. Thus the differential rate for fixed final kinetic energy, i.e., fixed $j-j'$, is expressed as a sum of the contributions of all channels,

$$\left[\frac{dw}{d\Omega}\right]_{j-j'}=\frac{(2m_e^3\omega^5)^{1/2}}{(2\pi)^2}(j-j'-E_b/\omega)^{1/2}\times\sum_{\text{ch}}(j-2z)^2|\Phi_i(\mathbf{P}_1)|^2_{\text{av}}\times(F_1^2+F_2^2)J_j^2(\zeta)J_{j'}^2(\zeta)\ . \quad (87)$$

Figures 5–7 show the numerical results by using this theory with intensities of 1×10^{13}, 2.1×10^{13}, and 4×10^{13} W/cm^2 per beam, respectively, to predict the angular distribution and comparisons with experimental results. The model atom is still xenon and the electron before ionization is in the $5p_{3/2}$ state. The photoelectron in the calculations has a kinetic energy of 5.4, 7.7, 10.0, 12.3, and 14.7 eV, corresponding to a net absorption of 15, 17, 19, 21, and 23 photons, respectively. In the figures the vertical lines are calculated results from this theory and the diamond-shaped points are experimental measurements by Bucksbaum and co-workers. Of the three calculated results of angular distributions in different laser intensities, the 2.1×10^{13} W/cm^2 beam intensity has the best fit

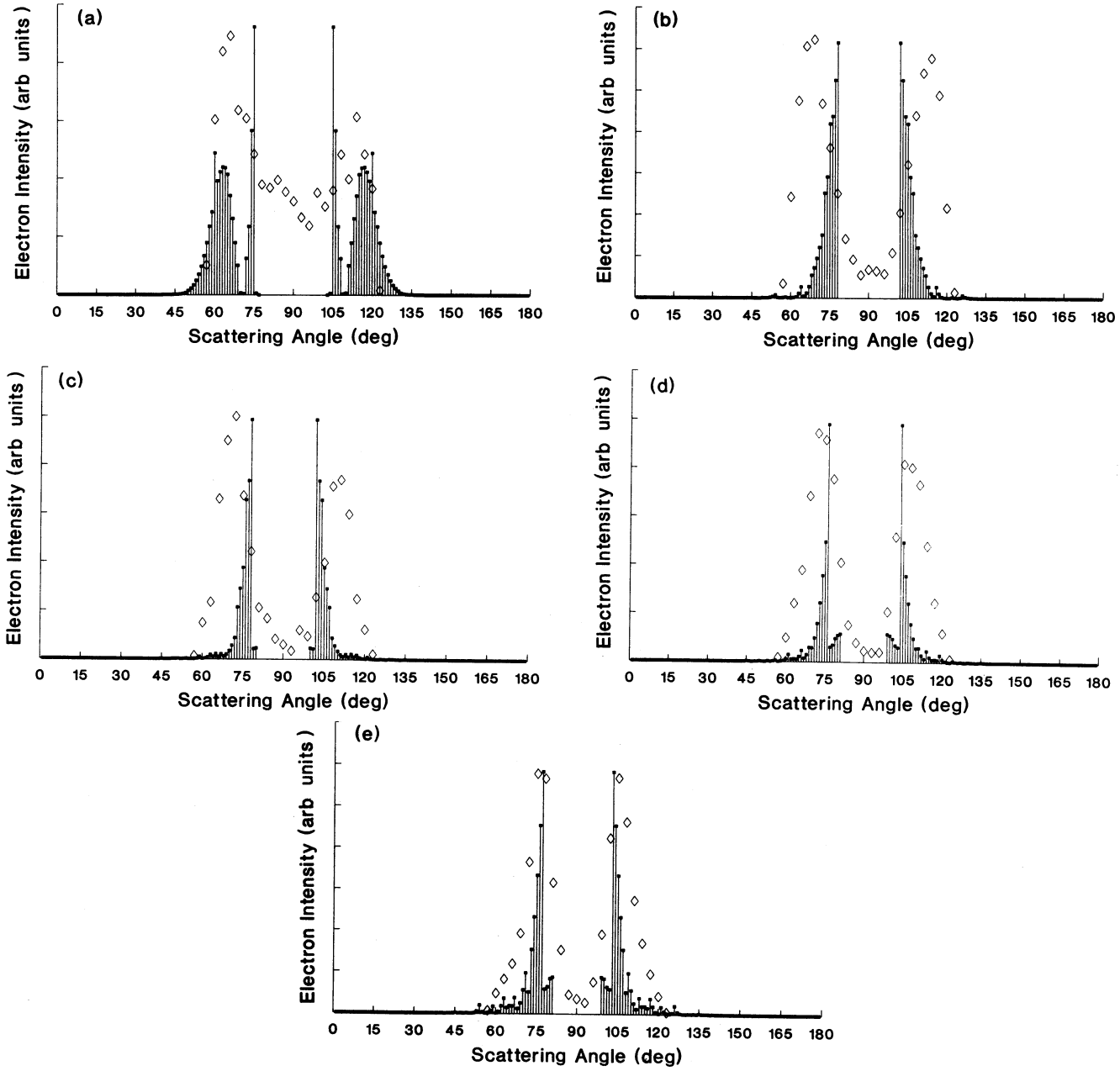

FIG. 7. Angular distributions for the photoelectron in the (a) 15-, (b) 17-, (c) 19-, (d) 21-, and (e) 23-photon ionization cases calculated at an intensity of 4×10^{13} W/cm^2 per beam and comparisons with the measurements (◇) of Bucksbaum and co-workers.

to the experimental data. This agrees with the estimated beam intensity of $(2–4)\times10^{13}$ W/cm^2 in the experiment by Bucksbaum [18]. In this theory, the energies of ponderomotive decay are always integers measured by the photon energy. As an electron moves in a 1064-nm standing-wave laser light with intensity 1×10^{13} W/cm^2 for each beam, the total ponderomotive potential energy $2z$ (measured by the photon energy) is 1.81. According to Eq. (69), there are two channels, $j'=0$ and 1, for multiphoton ionization. In the 15- and 23-photon processes there are two pairs of peaks, as shown by Fig. 5. The inner pairs correspond to the absorption of 16 and 24 photons, respectively, for ionization and emission of one photon for ponderomotive decay. The outer pairs correspond to the absorption of 15 and 23 photons directly for ionization and with no ponderomotive decay. In the latter case the electron gains the full ponderomotive potential, so the splitting angle is larger. Similar analysis can be made for the others, but the nonmonotonic property of the functions $J_j^2(\zeta)$ makes the line shapes of the angular distributions more complicated.

The fraction of ponderomotive energy kept by the photoelectron when it leaves the radiation field has been a long-standing question. Here, we can see the unique advantage of this theory, in which we sum the rates over all possibilities of pondermotive decay, rather than making an artificial assumption for it. Future experiments may observe the second pair of peaks and successive pairs of peaks in cases with a higher ponderomotive potential. The quantum nature of ponderomotive potential was mentioned in the GAC paper as a purely mathematical consequence. The successive pairs of angular-distribution peaks predicted by the current theory might be an observable quantum effect associated with the ponderomotive energy.

In our theory, the curve of angular-distribution splitting is sharp and emission of the photoelectron exactly between the peaks is forbidden, in contrast to the experimental measurements where the curves are much smoother. The reason is that in our theory we assume that the laser interaction is switched off adiabatically, while the actual switching-off process in experiments is nonadiabatic.

The mode-change quantum number in the current example is of the order 10^3, which means that the deflected photoelectron has absorbed about 500 photons from one mode, and emitted about another 500 photons to the other mode. The emission is a stimulated emission process. In this sense, the process observed by BSB is a Kapitza-Dirac effect—the strong-field Kapitza-Dirac effect. This kind of photon absorption and emission process is not due to the usual photon-electron interaction shown by Eq. (1). Rather, it is a scattering process due to the ponderomotive potential.

Case II. Two beams with the same helicity and opposite angular momentum. Using Eq. (39) to calculate the overlap factor in Eq. (61), we obtain

$$\langle\phi_f;m_1,m_2|\Psi_\mu\rangle=(2\pi)^3V_e^{-1}\delta(\mathbf{P}_\mu-\mathbf{P}-(j_1'-j_2')\mathbf{k})\times\mathcal{J}_{j_1'j_2'}(\zeta)^*e^{-i(j_1'-j_2')\varphi}\quad(j_1'\equiv m_1-n_1,j_2'\equiv m_2-n_2)\ . \tag{88}$$

Energy conservation is the same as for case I. From Eq. (63) we have

$$\frac{1}{2m_e}\mathbf{P}_\mu^2=\frac{\mathbf{P}^2}{2m_e}-(2z-j')\omega\ , \tag{89}$$

where j' is defined by Eq. (6) and satisfies

$$j'=j_1'+j_2'\ . \tag{90}$$

Momentum conservation from the δ function in Eq. (88) is

$$\mathbf{P}_\mu=\mathbf{P}-(j_2'-j_1')\mathbf{k}\ . \tag{91}$$

Equations (89) and (91) are exactly the same as Eqs. (63) and (64), except that m_2-m_1 is replaced by $j_2'-j_1'$. In the current xenon example, $|j_1'|$ and $|j_2'|$ must be around 500.

The transition-rate formula in case II is

$$\left[\frac{dw}{d\Omega}\right]_{j-j'}=(j-j'-E_b/\omega)^{1/2}\sum_{\text{ch}}\frac{(2m_e^3\omega^5)^{1/2}}{(2\pi)^2}(j_1+j_2-2z)^2|\Phi_i(\mathbf{P}-(j_1-j_2)\mathbf{k})|^2_{\text{av}}|\mathcal{J}_{j_1j_2}(\zeta)|^2|\mathcal{J}_{j_1'j_2'}(\zeta)|^2\ , \tag{92}$$

where $j=j_1+j_2$ and the sum is carried out such that $j-j'$ is a fixed number. Here we can see that unlike in case I, the stimulated emission and absorption of $|j_1'|$ and $|j_2'|$ photons are through the photon-electron interaction. Thus the transition rate in this case is proportional to the square of the generalized Bessel functions indexed by j_1' and j_2'. The Bessel functions and the generalized Bessel functions with indices around 500 are very small for $\zeta_1\sim1-10$ and $z\sim1-10$ for the above experimental conditions. So, large-angle deflections of the photoelectron are present, but the amplitude is too small to be observed.

V. CONCLUSIONS

Comparison between the two theories and experiment shows that the nonperturbative scattering states provide a better description of photoelectrons produced in high-intensity multiphoton-ionization processes than Volkov states provide. The Keldysh ansatz, which assumes Vol-

kov states as the final states for the electron in multiphoton ionization, is not adequate because the transition from the Volkov states to free states should be included, as shown by the scattering theory of GAC and its multimode extension. In our scattering theory, the multiphoton-ionization process partitions naturally into two subprocesses. The first subprocess is exactly the KFR process during which the electron is ionized from a bound state into the radiation field, while the second subprocess is the process of the photoelectron leaving the radiation field. Energy-momentum conservation in the second subprocess determines the angular-distribution splittings. Although the scattering theory of GAC contains the mechanism for the photoelectron leaving the radiation field, the single-mode assumption makes the theory incomplete. A complete theory should include all possible spontaneous-emission modes in addition to nonadiabatic switching, which would smear out the sharp valleys in the predicted angular distributions. However, aside from this, the predicted angular distributions show good qualitative agreement with the measurements. Also, the peak splitting in the angular distribution agrees well with the predicted $\sin(\pi/2-\theta_{\max})\propto 1/E^{1/2}$ law.

A quantized-field approach is necessary in two respects. First, the complete system of interacting atoms and photons is treated as an isolated system for which the total energy and momentum from the initial state via the intermediate states to the final state is well defined. Thus the evolution of the energy distribution among the electrons and photons due to interactions and energy transfers is well determined. This provides a useful guide to the formulation of the relevant energy-momentum conservation laws that govern, for example, the angular-distribution splittings. Second, high-intensity radiation fields are commonly thought of as classical fields, but this does not mean that there are no quantum effects in the classical-field regime. Above-threshold-ionization peaks spaced apart by one-photon energy show a quantum effect in strong radiation fields. Ponderomotive potential energy as a classical quantity is continuous, and significant only in strong radiation fields. Quantum effects associated with the ponderomotive potential might be observable in photoelectron angular-distribution peaks due to different ponderomotive-energy decays. These produce the fine structure in the angular-distribution peaks shown in the figures. They may be observable, provided that the adiabatic condition is sufficiently well satisfied. It would be interesting to search for them in future experiments.

ACKNOWLEDGMENTS

We would like to thank P. H. Bucksbaum for helpful discussions concerning his experiment. This work has been supported by the Natural Science and Engineering Research Council of Canada. One of us (G .W. F. D.) thanks the Killam Foundation for support.

APPENDIX

The factor F has an algebraically equivalent form

$$F=\sum_{n_2}\left[\frac{(m_1+m_2-n_2)!n_2!}{2^{m_1+m_2}m_1!m_2!}\right]^{1/2}\times\left[\sum_t(-1)^t\begin{bmatrix}m_1\\ n_2-t\end{bmatrix}\begin{bmatrix}m_2\\ t\end{bmatrix}\right]\times(-1)^{n_2/2}2^{-l}\left[\begin{bmatrix}2l-n_2\\ l-n_2/2\end{bmatrix}\begin{bmatrix}n_2\\ n_2/2\end{bmatrix}\right]^{1/2}. \quad \text{(A1)}$$

In the sum, n_2 runs over all even numbers. The factor in the middle can be changed by using a combinatorial identity

$$\sum_t(-1)^t\begin{bmatrix}m_1\\ 2s-t\end{bmatrix}\begin{bmatrix}m_1+\Delta\\ t\end{bmatrix}=(-1)^s\sum_p(-1)^p\begin{bmatrix}\Delta\\ 2p\end{bmatrix}\begin{bmatrix}m_1\\ s-p\end{bmatrix}, \quad \text{(A2)}$$

which can be proven by using a generating function technique

$$\sum_s\sum_t(-1)^t\begin{bmatrix}m_1\\ 2s-t\end{bmatrix}\begin{bmatrix}m_1+\Delta\\ t\end{bmatrix}x^{2s}=(1-x^2)^{m_1}[(1+x)^\Delta+(1-x)^\Delta]/2=\sum_s\sum_p(-1)^{s-p}\begin{bmatrix}\Delta\\ 2p\end{bmatrix}\begin{bmatrix}m_1\\ s-p\end{bmatrix}x^{2s}. \quad \text{(A3)}$$

Here we have assumed that Δ is a positive integer. Since we can always switch the names of the two modes, the assumption does not affect the final conclusion. Now, F is in a form

$$F=\sum_{n_2}\left[\frac{(m_1+m_2-n_2)!n_2!}{2^{m_1+m_2}m_1!m_2!}\right]^{1/2}\times\left[\sum_p(-1)^p\begin{bmatrix}\Delta\\ 2p\end{bmatrix}\begin{bmatrix}m_1\\ \frac{1}{2}n_2-p\end{bmatrix}\right]\times 2^{-l}\left[\begin{bmatrix}2l-n_2\\ l-n_2/2\end{bmatrix}\begin{bmatrix}n_2\\ n_2/2\end{bmatrix}\right]^{1/2}. \quad \text{(A4)}$$

In the large-photon-number limit, the mode-change quantum number Δ as well as the transferred photon numbers are all much smaller than the background-photon numbers. Thus we have

$$0\le s\le\Delta\ll m_1\approx l,\quad 0\le j-j'\ll m_1\approx l. \quad \text{(A5)}$$

By the first relation of Eq. (A5), we can simplify the middle factor of Eq. (A4) by applying Stirling's formula. The result is

$$\sum_p (-1)^p \begin{bmatrix} \Delta \\ 2p \end{bmatrix} \begin{bmatrix} m_1 \\ \frac{1}{2}n_2 - p \end{bmatrix} \approx \begin{bmatrix} m_1 \\ \frac{1}{2}n_2 \end{bmatrix} \sum_p (-1)^p \begin{bmatrix} \Delta \\ 2p \end{bmatrix} \left[\frac{n_2}{2m_1 - n_2} \right]^p \approx \begin{bmatrix} m_1 \\ \frac{1}{2}n_2 \end{bmatrix} \sum_p (-1)^p \begin{bmatrix} \Delta \\ 2p \end{bmatrix} \left[\frac{n_2}{2l - n_2} \right]^p . \quad \text{(A6)}$$

The sum can be carried out exactly,

$$\sum_p (-1)^p \begin{bmatrix} \Delta \\ 2p \end{bmatrix} \left[\frac{n_2}{2l - n_2} \right]^p = \left[\frac{2l}{2l - n_2} \right]^{\Delta/2} \cos(\Delta\gamma) , \quad \text{(A7)}$$

where

$$\gamma = \arccos \left[\frac{2l - n_2}{2l} \right]^{1/2} . \quad \text{(A8)}$$

By Eq. (A5), we can combine the first factor of Eq. (A4) with the first factor of the right-hand side of Eq. (A6),

$$\left[\frac{(m_1 + m_2 - n_2)! n_2!}{2^{m_1+m_2} m_1! m_2!} \right]^{1/2} \begin{bmatrix} m_1 \\ \frac{1}{2}n_2 \end{bmatrix} \approx 2^{-l} \left[\begin{bmatrix} 2l - n_2 \\ l - n_2/2 \end{bmatrix} \begin{bmatrix} n_2 \\ n_2/2 \end{bmatrix} \right]^{1/2} \left[\frac{2l - n_2}{2l} \right]^{\Delta/2} . \quad \text{(A9)}$$

The factor F simplifies to

$$F \approx 2^{-2l} \sum_{n_2} \begin{bmatrix} 2l - n_2 \\ l - n_2/2 \end{bmatrix} \begin{bmatrix} n_2 \\ n_2/2 \end{bmatrix} \cos(\Delta\gamma) . \quad \text{(A10)}$$

The sum can be approximated by an integration. The accuracy of the integral approximation can be checked in the $\Delta = 0$ case. By applying Stirling's formula, we have

$$2^{-2l} \sum_{n_2} \begin{bmatrix} 2l - n_2 \\ l - n_2/2 \end{bmatrix} \begin{bmatrix} n_2 \\ n_2/2 \end{bmatrix} \approx \pi^{-1} \int_0^l \frac{dx}{(l-x)^{1/2} x^{1/2}} = 1 , \quad \text{(A11)}$$

which is exactly the same as the result of the direct summation shown by Eq. (52). With this confidence, we write Eq. (A10) in the integral form

$$F \approx \pi^{-1} \int_0^l \frac{dx}{(l-x)^{1/2} x^{1/2}} \cos \left[\Delta \cos^{-1} \left[\frac{l-x}{l} \right]^{1/2} \right] . \quad \text{(A12)}$$

After rescaling and changing the variable, the above integral can be simplified without any further approximation. Thus we have

$$F \approx 2\pi^{-1} \int_0^{\pi/2} \cos(\Delta\gamma) d\gamma = \begin{cases} 1 & \text{if } \Delta = 0 \\ 0 & \text{if } \Delta = \text{even} \\ \pm 2/\pi\Delta & \text{if } \Delta = \text{odd} . \end{cases} \quad \text{(A13)}$$

The first case corresponds to the KFR case, where there is no mode-change quantum number. In the second case, there is no transition. The only possible case is the third case, where Δ is obtained by solving Eq. (70). Indeed, one can take an odd number for Δ, which is closest to the exact value. The sign in front of the third case removes the sign assumption made in the proof. Thus the limiting form of F is proven.

[1] P. H. Bucksbaum, D. W. Schumacher, and M. Bashkansky, Phys. Rev. Lett. **61**, 1162 (1988).

[2] P. L. Kapitza and P. A. M. Dirac, Proc. Cambridge Philos. Soc. **29**, 297 (1933).

[3] G. S. Voronov and N. B. Delone, Zh. Eksp. Teor. Fiz. **50**, 78 (1966) [Sov. Phys. JETP **23**, 54 (1966)].

[4] L. V. Keldysh, Zh. Eksp. Teor. Fiz. **47**, 1945 (1964) [Sov. Phys. JETP **20**, 1307 (1965)].

[5] F. H. M. Faisal, J. Phys. B **6**, L89 (1973).

[6] H. R. Reiss, Phys. Rev. A **22**, 1786 (1980).

[7] H. S. Antunes Neto and L. Davidovich, Phys. Lett. **53**, 2238 (1984); P. W. Milonni, Phys. Rev. A **38**, 2682 (1988); J. Javanainen and J. H. Eberly, *ibid.* **39**, 458 (1989).

[8] M. Bashkansky, P. H. Bucksbaum, and D. W. Schumacher, Phys. Rev. Lett. **59**, 274 (1987); R. R. Freeman and P. H. Bucksbaum, J. Phys. B **24**, 325 (1991).

[9] W. Becker, R. R. Schlicher, and M. O. Scully, J. Phys. B **19**, L785 (1986); K. Unnikrishnan, *ibid.* **23**, L541 (1990).

[10] D. S. Guo, T. Åberg, and B. Crasemann, Phys. Rev. A **40**, 4997 (1989).

[11] T. Åberg, D. S. Guo, J. Ruscheinski, and B. Crasemann, Phys. Rev. A **44**, 3169 (1991).

[12] X. Mu, Phys. Rev. A **42**, 2944 (1990); X. Mu, J. Ruscheinski, and B. Crasemann, *ibid.* **42**, 2949 (1990).

[13] D. S. Guo and G. W. F. Drake, J. Phys. A (to be published).

[14] D. S. Guo, Phys. Rev. A **42**, 4302 (1990).

[15] D. S. Guo and T. Åberg, J. Phys. A **21**, 4577 (1988).

[16] J. Riordan, *Combinatorial Identities* (Wiley, New York, 1968), p. 130.

[17] T. Tietz, J. Chem. Phys. **22**, 2094 (1954).

[18] P. H. Bucksbaum (private communication).